

# New Method for Robust Analysis of Critical Behavior of Magnetic Systems

Harish Chandr Chauhan,<sup>1</sup> Umesh C. Roy,<sup>2</sup> Shovan Dan,<sup>3</sup> A. Thamizhavel,<sup>3</sup> and Pintu Das<sup>1</sup>

<sup>1</sup>*Department of Physics, Indian Institute of Technology Delhi, New Delhi 110016, India\**

<sup>2</sup>*Department of Chemistry, College of Staten Island, Staten Island, NY 10314, USA*

<sup>3</sup>*Department of Condensed Matter Physics and Materials Science,*

*Tata Institute of Fundamental Research, Homi Bhabha Road, Colaba, Mumbai 400005, India*

Here, we present new methods for critical analysis to determine the range of exchange interaction(s) and appropriate values of critical exponents for different magnetic systems. From computational and experimental investigations of magnetic behavior of Ni and Gd, we show that the critical behavior remains the same on either side of transition temperature. Using our proposed method of analysis for Gd, we find a critical role of competing interactions where the local electron moments follow 3D Ising type short-range interactions whereas the itinerant electron moments constitute mean-field type long-range RKKY interaction.

In the studies of phase transitions for cases, such as condensation of gases, melting of solids, magnetic ordering in solids, etc., the understanding of the behavior of the systems adjacent to the critical point is of fundamental interest [1–3]. Generally, the physics of phase transition is governed by the behavior of the microscopic constituents which interact strongly in a cooperative fashion. Critical exponents (CEs), which define the power law behavior of physical quantities exhibiting singularities at the critical points, indicate the qualitative nature, i.e., the critical behavior of a system [4, 5]. The types of cooperative interactions (short-range, long-range, etc.) among the constituent entities play a significant role in defining the CEs. In a magnetic system, the magnetic moments are known to interact typically via different exchange interactions resulting in a set of CEs [6–13]. Different methodologies have been suggested for determination of a set of CEs ( $\alpha, \beta, \gamma, \delta$ , etc.) corresponding to physical quantities such as specific heat ( $C_v$ ), spontaneous magnetization ( $M$ ), susceptibility ( $\chi$ ) and magnetization isotherm recorded at the paramagnetic transition temperature ( $T_C$ ), respectively for various universality classes (UCs), viz., Heisenberg, XY, Ising, mean field (MF), or tricritical MF [4, 5]. The CEs are mutually related and they depend critically on the dimensionality (of space and spin) and the range of microscopic interactions. Although, most methodologies suggest same CEs for two sides of a transition, a recent theoretical work suggested otherwise [14]. In fact, the recent proposal [15] based on a modified Arrott-plot (MAP) [16] analysis of a magnetic system with competing interactions (hereafter, referred as nontrivial system) suggested different CEs on either side of  $T_C$ .

Several groups have determined CEs for numerous nontrivial magnetic systems, such as  $\text{La}_{0.6}\text{Ag}_{0.2}\text{Bi}_{0.2}\text{MnO}_3$  [7],  $\text{La}_{0.7}\text{Sr}_{0.3}\text{MnO}_3$  [17],  $\text{Co}_{3.6}\text{Fe}_{4.4}\text{Zn}_8\text{Mn}_4$  [18],  $\text{La}_{0.75}\text{Sr}_{0.25}\text{MnO}_3$  [19], and Gd [20–23], using the existing methodologies. It was highlighted that the reported CE values do not belong to any single UC [7, 17–20]. No correlation of the reported values of CEs with the known competing interactions, eg. super-exchange,

double-exchange, dipolar, Ruderman-Kittel-Kasuya-Yusida (RKKY), etc., in nontrivial systems [6–13] raises a serious question: is the fundamental understanding of the critical behavior or the used methodologies or both the factors responsible for this?

It has been pointed out that the established methodologies such as iteration method (IM) [16], Kouval-Fisher plots [24], and entropy analysis [25], may yield ambiguous values of the CEs. Additionally, the determined value of  $\gamma$  is essentially used to determine  $\sigma$  [26] which defines the existing range of interaction in a magnetic system. The theoretical suggestions for long- and short-range interactions correspond to  $\sigma \leq 1.5$  and  $\sigma \geq 2.0$ , respectively, often leads to conflicting interpretations, particularly when  $\sigma$  falls between the two values [4, 5, 18, 27–29]. Furthermore, the  $\gamma$  for a nontrivial magnetic system constitutes the effective value. So, an inaccurate determination of  $\sigma$ , which effectively depends on  $\gamma$  [26], may result in non-physical conclusions.

Thus, we are still left with several open problems which are necessary to resolve for better understanding of the physics of critical behavior. Some of them are as follows: There is no methodology to (i) accurately identify the range of competing interactions in nontrivial systems and their resultant effect in presence of applied magnetic field ( $B = \mu_0 H$ ), and (ii) systematically determine accurate and convergent values of CEs in least number of iterations. It is still unknown if the competing short- and long-range interactions constitute different UCs. Whether the two sets of exponents on either side of  $T_C$  are due to the intrinsic complex interactions or due to technical issues in the methodologies used for the analysis of magnetic behavior requires a thorough investigation.

In this letter, we present our computational and experimental investigations on the phase transition and the critical phenomena. We report the: (i) the development of robust methodologies to determine precise and accurate values of the CEs in least number of iterations, (ii) the effect of  $B$  on the nature of the competing interactions in nontrivial systems, and (iii) why the values of the CEs determined for nontrivial systems do not belong

to a single UC. By performing computational investigations for trivial system, such as Ni, we first show that the iteration method may lead to ambiguous results. We then propose a method to identify the range of exchange interaction. Next, we propose new methodologies using the computationally simulated magnetization isotherms to determine correct and convergent values of the CEs in least number of iterations. Subsequently, we show that magnetic systems hold identical values of the CEs on either side of  $T_C$ . Finally, by performing experimental investigations for single crystals of Gd, we show that the CEs for nontrivial systems do not belong to a single UC due to the competing effect of the existing exchange interactions.

In order to determine precise values of CEs, we first proceed with the analysis of the magnetization ( $M$ ) data for Ni. The  $T$ -dependent magnetization ( $M - T$ ) for both zero- and applied- $B$  are determined by carrying out atomistic simulations based on solution of Landau-Lifshitz-Gilbert equation using Vampire simulation package [30, 31].  $T_C = 655$  K is determined from the minima of the first-derivative [inset of Fig. 1(a)] of the  $M$  vs.  $T$  plot [Fig. 1(a)]. Using the relations,  $M \propto |\epsilon|^\beta$ ,  $M \propto (\mu_0 H)^\frac{1}{\delta}$  at  $T = T_C$  and the Widom relation  $\delta = 1 + \frac{\gamma}{\beta}$  [4, 5, 32, 33], we find  $\beta = 0.344(2)$  [Fig. 1(a)],  $\delta = 4.822(2)$  [Fig. 1(b)] and  $\gamma = 1.315(8)$ , respectively. Here,  $\epsilon = \frac{T - T_C}{T_C}$  is the reduced  $T$ . We denote the above methods of determination of CEs as the standard procedure (SP). We further define the normalized slopes ( $NS$ s) as the ratio of slope of the MAP at a given  $T$  and that at  $T_C$ , see [Fig. 1(c)].  $NS$ s  $\sim 1$  thus obtained for  $T \leq T_C$  [Fig. 1(d)] [31] confirms the reliability of the obtained values of CEs that belongs to 3D XY UC [34–38]. However, the values of CEs obtained by IM, viz.,  $\beta = 0.362(1)$  and  $\gamma = 1.222(10)$ , are different [Fig. 1(e)] suggesting that IM [31] is not yielding the correct values of the CEs. Moreover, the values of  $NS$ s, plotted using CE values obtained by IM, show deviation from 1 on either side of  $T_C$ , demonstrating further that IM is an incorrect approach to determine CEs. Additionally, the CEs determined using MIM for  $T \leq T_C$  shows 3D XY type short-range ( $\sigma \approx 2$ ) [31] interaction and  $NS \sim 1$  [18]. However, appropriate values of CEs for  $T \geq T_C$  could not be determined using MIM since  $NS$ s do not come close to 1 for the used  $T$ -range. Further, we note that in many real systems, SP may not be always applicable for critical analysis, see discussions below. Therefore, we propose novel methodologies for critical analysis as follows.

Figure 1(f) shows the plots of the  $T$ -dependence of intercepts obtained from the linear fits for MAPs corresponding to different UCs. Remarkably, we find that the intercepts estimated by both SP as well as by using the CEs of short-range standard UCs show a crossover at  $T \sim T_C$ . Interestingly, if CEs are estimated consid-

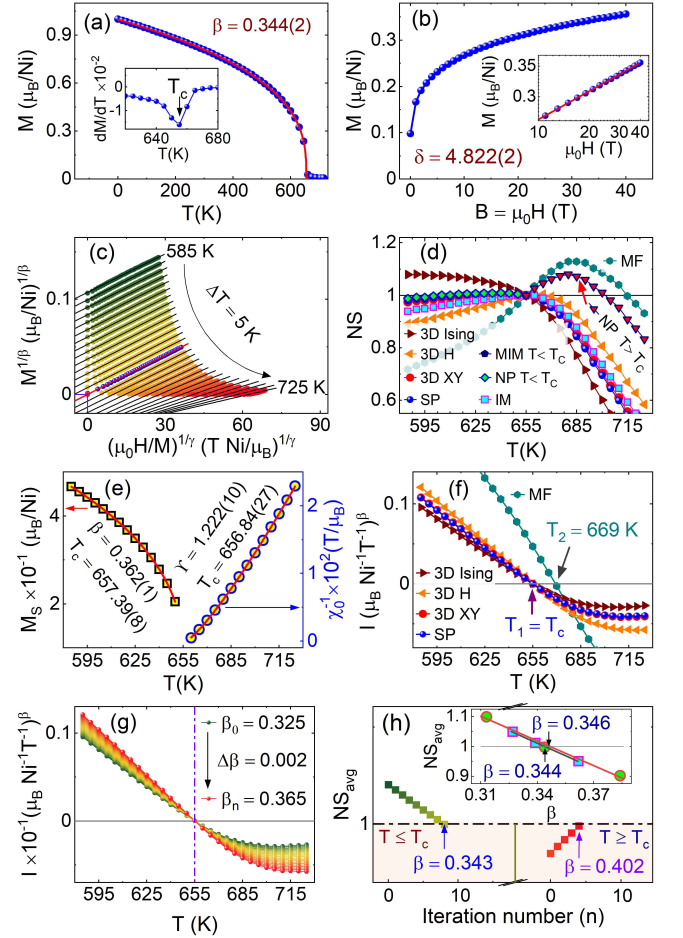


Figure 1. (a) The temperature-dependent magnetization ( $M - T$ ) plot obtained from the Vampire atomistic simulation for monatomic Ni. Inset of (a) represents the first derivative of the  $M - T$  resulting  $T_C = 655$  K. (b) Field-dependent magnetization ( $M - H$ ) estimated at  $T = T_C$ . Inset of (b) represents the linear fit to log-log plot of  $M - H$ . (c) The modified Arrott-plots constructed using the critical exponents determined from standard procedure. (d) Normalized slope ( $NS$ ) vs.  $T$  plots constructed using the CEs of the standard UCs, and the CEs determined from IM, MIM, SP and new proposal (NP). (e) The plots of  $M_S$  and  $\chi_0^{-1}$  against  $T$ . Symbols represent simulated data while solid lines are fit to respective curves. (f) intercept ( $I$ ) vs.  $T$  plots constructed using the CEs determined using SP and of standard UCs. (g)  $I$  vs.  $T$  plots for different values of  $\beta$  and  $\gamma$  which are related as  $\gamma = \beta \times (\delta - 1)$ . (h) Variation of  $NS_{avg}$  with  $n$  which is related with  $\beta$  as  $\beta(n) = \beta_i + \Delta\beta \times n$ . Inset of (h) represent the  $NS_{avg}$  vs.  $\beta$  plots constructed using few sets of  $\beta$  and corresponding  $\gamma$  as mentioned in (g). MF: mean field, TMF: tricritical MF and H: Heisenberg.

ering MF UC representing a long-range interaction, the crossover  $T$  ( $T_2 = 669$  K) is found to deviate from  $T_C$ . Thus, from the detailed analysis of CEs for Ni, we identify the approach of intercept analysis as a reliable method to determine the short-range interaction in Ni for which we computationally determine the  $M - H$  isotherms by

considering anisotropy value as zero. The same approach may also be applicable to identify long-range interactions if the intercepts, determined using the CEs of MF UC, show a crossover around  $T_C$  (see discussions below). This suggests that the new method of intercept analysis may be a proper approach to determine the range of interactions. By using this approach, we demonstrate (see below) the role of itinerant electrons in the magnetic behavior of Gd. Intriguingly, we note further that the different values of  $\beta$  and  $\gamma$  corresponding to short-range standard UCs lead to the same value of  $\delta$  which is equal to the  $\delta$  [Fig. 1(b)] as determined from the  $M-H$  at  $T_C$ . Additionally, the values of the intercepts determined using the CEs of 3D Ising, 3D XY, 3D Heisenberg and SP converge to 0 at  $T = T_C$  (the crossover  $T$ ). This suggests that the values of CEs related with  $\delta$  may lead to value of intercept  $\approx 0$  at  $T = T_C$  for multiple set of  $\beta$  and  $\gamma$ .

Using the above information, we now describe our new proposal for critical analysis as follows. We vary  $\beta$  in a controlled way as  $\beta(n) = \beta_i \pm \Delta\beta \times n$ , where  $\beta_i$  is the initially selected value of  $\beta$ ,  $\Delta\beta$  is the increment in  $\beta$  for each iteration and  $n$  is the iteration number.  $\beta_i$  can be chosen as belonging to a standard UC or a random value with the condition that the chosen set of  $\beta$  and corresponding  $\gamma$  lead to quasi-linear behavior of MAPs. The corresponding values of  $\gamma$  are determined for each  $\beta(n)$  using the Widom relation [33] as  $\gamma = \beta(n) \times (\delta - 1)$ , where  $\delta$  is directly obtained from  $M-H$  curve at  $T = T_C$  [Fig. 1(b)]. The intercepts of MAPs thus obtained are found to exhibit a crossover at  $T_C$  [Fig. 1(g)] for multiple sets of  $\beta$  and  $\gamma$  values. In order to determine appropriate values of  $\beta$  and  $\gamma$ , the MAPs obtained as above are used to estimate an average value ( $NS_{\text{avg}}$ ) of  $NS$ s for  $T \leq T_C$  and  $T \geq T_C$  separately.  $NS_{\text{avg}}$  is defined by  $NS_{\text{avg}} = \frac{\sum_{i=1}^N (NS)_i}{N}$ , where  $i$  denotes the  $M-H$  isotherm at a given  $T$  and  $N$  is the total number of the isotherms appearing in the calculation. The  $NS_{\text{avg}}$  thus determined for each iteration  $n$  are plotted in Fig. 1(h). According to our proposal, the set of values of  $\beta$ ,  $\delta$  and  $\gamma$  corresponding to  $NS_{\text{avg}} = 1$  are the appropriate values of the CEs for a system. Remarkably, using our proposal for  $T \leq T_C$ , we determine  $\beta = 0.343(3)$  and  $\gamma = 1.311(18)$  which are consistent with the CEs obtained using the SP. The error in  $\beta$  is manually controllable while the error in  $\gamma$  depends on the imposed error in  $\beta$  and the error appearing in  $\delta$ . In the above proposal, we vary  $\beta$  and  $\gamma$  in iterative way. However, we propose another unconventional and much simpler approach to determine appropriate values of CEs as follows [31]. Select at least three sets of  $\beta$  and corresponding  $\gamma$  such that the estimated  $NS_{\text{avg}}$  falls within  $1 \pm 0.05$ . One can extend or reduce the above defined range for  $NS_{\text{avg}}$  within the range of linear variation of the  $NS_{\text{avg}}$  vs.  $\beta$  plot [31], see the inset of Fig. 1(h). Thus, using the *intercept* and *slope*, determined from the linear fit to  $NS_{\text{avg}}$  vs.  $\beta$  plot, one can directly esti-

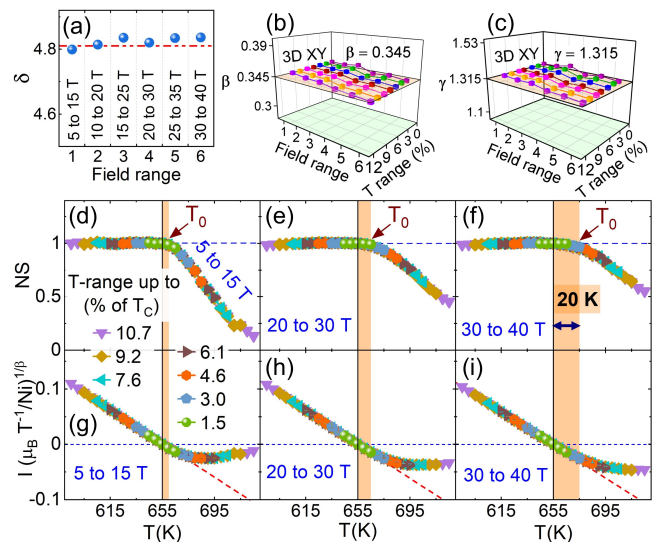


Figure 2. (a) The field-dependent variation of  $\delta$  estimated for different applied magnetic field ( $B$ ) ranges as mentioned. (b) and (c) represent the variation of  $\beta$  and  $\gamma$ , respectively, for different  $B$  and temperature ( $T$ ) ranges determined using our new proposal (NP). The  $T$  ranges are mentioned in below Figs. (d)–(i). (d)–(f) and (g)–(i) represent  $NS$  and intercept ( $I$ ) against  $T$  plots, respectively, constructed using the CEs obtained using NP for different  $B$  and  $T$  ranges.

mate  $\beta = \frac{1 - \text{intercept}}{\text{slope}}$  and  $\gamma = \frac{1 - \text{intercept}}{\text{slope}} \times (\delta - 1)$  [31]. The  $\beta = 0.344(3)$  and  $\gamma = 1.315(18)$  thus obtained are the same as the values of CEs determined using SP.

However, for  $T \geq T_C$ , we find that the values of CEs ( $\beta = 0.402(5)$  and  $\gamma = 1.533(20)$ ) resulting  $NS_{\text{avg}} \sim 1$  are significantly different than as obtained for  $T \leq T_C$ , see Fig. 1(h). As our new approach shows that for  $T \leq T_C$  the CE values are consistent with that obtained by the SP and  $NS \sim 1$ , whereas for  $T \geq T_C$ , the  $NS$  values are significantly different from 1 [Fig. 1(d)], it suggests that the CEs obtained for  $T \geq T_C$  do not define the actual critical behavior. This is further supported from  $\beta$  which is undefined for above  $T_C$  [32]. We infer that the consideration of identical range of  $T$  for below and above  $T_C$  may have resulted to such discrepancy. In the following, we verify this and discuss our proposal for the estimation of appropriate range of  $T$  and  $B$  for below and above  $T_C$  for critical analysis.

Figures 2(a, b, c) show the analysis of the behavior of  $\delta$ ,  $\beta$  and  $\gamma$  in different ranges of  $T$  and  $B$  as determined using our proposed method as described above for  $T \leq T_C$ . In Figs. 2(b-i), seven different  $T$  ranges of 10.7% to 1.5% of  $T_C$  are considered. We find that the CEs thus obtained are robust across different  $T$  (for  $T \leq T_C$ ) and  $B$  ranges clearly suggesting that the critical behavior associated with local electron moments (here, the modeled Ni system) is independent of  $B$ . The CE values thus determined correspond to the standard UC of 3D XY. We next proceed to determine the appropriate

range of  $T$  for  $T > T_C$  as follows. Figures 2 (d-f) show the representative plots of NSs, calculated from MAPs using the robust values of CEs obtained using the proposed method for  $T \leq T_C$ . For brevity, three different  $B$  ranges, viz., 5-15 T, 20-30 T and 30-40 T, respectively, are shown. Clearly, for  $T \leq T_C$ , the  $NS \sim 1$  for the entire  $T$  range. However, for  $T > T_C$ , we observe that the values deviate from  $NS \sim 1$  beyond  $T = T_0$  [Fig. 2(d)] which is very close to  $T_C$ . Interestingly, the  $T$ -range, *i.e.*,  $T_0 - T_C$  for  $T > T_C$  showing  $NS \sim 1$  grows with increasing  $B$  [Figs. 2(e and f)]. We, therefore, propose a process to determine the appropriate ranges of  $T$  and  $B$  for critical analysis. Selecting the  $M - H$  isotherms at relatively high- $B$  and low- $T$  ranges,  $NS$ s are to be determined using the  $\beta$  and corresponding  $\gamma$  as we proposed above. The maximum  $T$ -range for the chosen  $B$  range showing  $NS \sim 1$  will be the appropriate range to be considered for the critical analysis. It is to be noted that the field-dependent critical analysis is required if  $\delta$  varies with  $B$ . Furthermore, as we verify the behavior of linearity of  $NS$ s with  $T$  [Figs.2(g-i)], we find that the range of linearity of the intercepts also increases with increasing  $B$ -range confirming the identical critical behavior on either side of  $T_C$ . We thus show that the appropriate  $T$ -range can also be determined from the plot of intercepts vs.  $T$  showing the linear behavior.

Using our proposed methods for critical analysis, we next carry out to investigate the role of itinerant electron magnetism on the critical behavior emerging in Gd. Although the magnetic properties of this rare earth material is interesting for applications, however, the exact nature of the interactions leading to the observed magnetic behavior of Gd remains unclear [10, 39–42]. The complex competing interactions between local  $4f$  as well as itinerant electrons makes Gd an interesting “nontrivial” system [39–42]. The previous studies for critical behavior of Gd report conflicting conclusions [20–23]. From  $B$ -dependent studies, it was suggested that the 3D Heisenberg UC in low- $B$  changes to 3D Ising in the high- $B$  [23]. However, the values of  $\gamma$  and  $\delta$  reported for low- $B$  range do not fully justify the claim. Intriguingly, although the role of long-range RKKY interaction involving itinerant electrons was suggested for Gd [8, 10], so far the analysis of critical behavior using existing methods indicated the presence of short-range interactions only [20–23].

We use high-quality single crystalline Gd in hexagonal close packed form, grown by Czochralski method [43], for the critical analysis [31]. The magnetization ( $M - T$  and  $M - H$ ) measurements were carried out in a SQUID setup (make: Quantum Design) by applying  $B$  along [0001] [31]. The  $T_C$  for the crystal is 292.4 K [Fig. 3(a)], and the magnetic moment per Gd atom is found to be  $\approx 7.63 \mu_B$  which is consistent with the values reported in literature [44]. The unusual feature observed near  $T_C$  in  $M - T$  plot [Fig. 3(a)] is ascribed to the competing energies in the system [10, 39–42]. Due to this, determi-

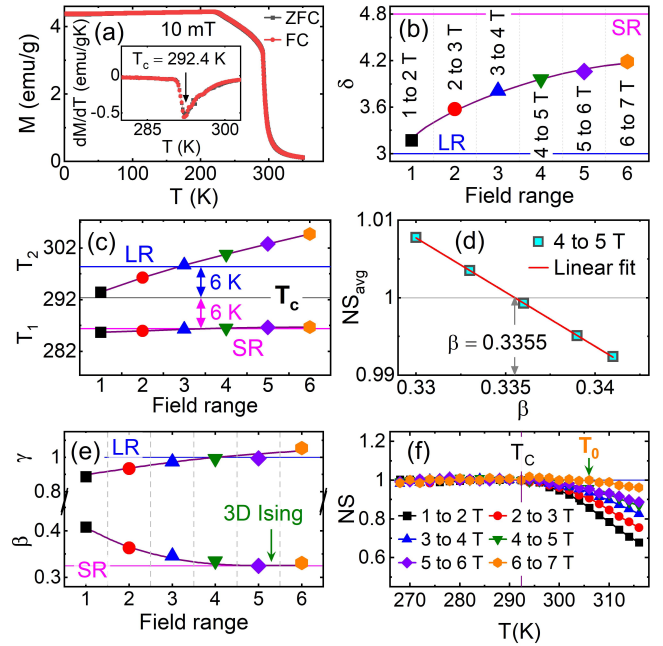


Figure 3. (a) The  $M - T$  recorded for Gd in field-cooled (FC) and zero-field-cooled (ZFC) warming modes by applying 10 mT of magnetic field along [0001]. Inset is the first-derivative of  $M - T$  which yields  $T_C = 292.4$  K. (b) The field-dependent variation of  $\delta_{MH}$ , estimated for different applied magnetic field ( $B$ ) ranges as mentioned. (c) Variation of  $T_1$  and  $T_2$  which constitute the crossover temperature  $T$  for the intercepts which are obtained from the linear fit to MAPs created using the  $\beta$  and  $\gamma$  of short-range 3D standard UCs and MF UC, respectively. (d) Variation of  $NS_{avg}$  vs.  $\beta$  to estimate appropriate  $\beta$  and  $\gamma$  associated with Gd in the  $B$ -range from 4 to 5 T. (e) Variation of  $\beta$  and  $\gamma$ , determined using our proposal, for different  $B$  ranges. (f)  $NS$  vs.  $T$  plots, constructed using the CEs obtained using our proposal, for different  $B$  ranges. SR: short-range, LR: long-range.

nation of  $\beta$  using SP [Figs. 1(a) and 1(b)] is not straight forward. Therefore, we use our proposed methods for critical analysis as follows. Unlike for Ni [Fig. 2(a)], our results for Gd clearly show a variation of  $\delta$  with  $B$ , see Fig. 3(b). The range of  $\delta$  observed in this case covers nearly the values for long-range MF to that for short-range standard UCs. So, we proceed for  $B$ -dependent critical analysis by considering 8% of  $T_C$  as the appropriate  $T$  range. The intercepts of the linear fit to MAPs, constructed using the CEs for short-range standard UCs as well as long-range MF UC, when plotted against the corresponding temperatures exhibit a crossover at  $T_1$  and  $T_2$ , respectively [Fig. 3(c)] [31]. See Fig. 1(f) for corresponding plots for Ni. According to our proposal, the intercepts of MAPs obtained using CEs of either short-range UCs or long-range MF UC exhibiting a crossover at  $T_C$  would determine whether the system has a short-range or a long-range interaction, respectively. Thus, our analysis showing  $T_2 \sim T_C$  at low- $B$  and deviating away

from  $T_C$  at high- $B$  suggests that the long-range interactions emerging due to itinerant electron moments becomes weaker with  $B$ . On the other hand,  $T_1$  starting at about 6 K away from  $T_C$  [Fig. 3(c)] in the low- $B$  range remains almost constant in the entire measured range of  $B$  suggesting that at high- $B$ , the nature of interactions are predominantly of short-range. This highlights the  $B$ -dependence of magnetic interactions in Gd.

Interestingly, independent analysis of CEs for Gd using our new approach shows results [Figs. 3(d) and 3(e)] which are consistent with that obtained from the intercept analyses. Whereas in low- $B$  range  $\beta$  and  $\delta$  suggest dominance of MF type long-range interaction, for high- $B$  the values suggest the interaction predominantly of 3D-Ising type short-range nature, see Figs. 3(b) and 3(e). Moreover,  $\gamma$  is found to remain  $\sim 1$  in the entire measured range of  $B$  [Fig. 3(e)] indicating the role of a complex competing interaction in Gd. Hence, our new approach based on the analysis of intercepts as well as CEs clearly identifies the competing role of short- and long-range interactions in different  $B$ -ranges in Gd. We argue that the local Gd moments interact via 3D Ising type short-range interaction while the presence of itinerant electrons results in MF type long-range RKKY interaction. We note that the CEs for typical magnetic systems, exhibiting competing interactions resulting in the unusual magnetic behavior, do not fall in a single UC [6, 7, 12, 13]. These observations eventually support our new findings. We again check the robustness and reliability of the obtained CE values (for  $T \leq T_C$ ) for Gd from the  $NS$  plots which show  $NS \sim 1$  in the entire  $T \leq T_C$  and in a small range of  $T$  above  $T_C$ , see Fig. 3(f). Similar to the case of Ni, the range of  $T$  showing  $NS \sim 1$  beyond  $T_C$  grows with  $B$  indicating further that the critical behavior remains same on either side of  $T_C$ .

In conclusion, we propose novel approaches to determine two important parameters for the analysis of critical behavior of magnetic systems, viz., the range of interactions and the values of CEs. We demonstrate the successful application of the methods for two magnetic systems, viz. Ni and Gd. By analyzing the intercepts of MAPs, we appropriately identify the range of exchange interaction in a system. From computational and experimental investigations of the critical behavior of Ni and Gd, we claim that  $NSs \sim 1$  for all  $M - H$  isotherms for  $T \leq T_C$  is the necessary and sufficient condition to test the reliability and robustness of the values of the CEs as determined by our proposed method. We argue that the *nontrivial* magnetic systems with competing interactions may simultaneously exhibit two types of UCs resulting in effective values of CEs. Our investigations show that the strength of short-range interaction among local moments remains same while the RKKY type long-range interaction emerging in Gd, due to the involvement of itinerant electron moments, weakens with increasing  $B$ . These investigations thus solve the long-standing problem of the

values of CEs not belonging to any specific UC observed for nontrivial systems. Our proposed methods may, thus, enable detailed understanding of critical behavior of magnetic systems.

## ACKNOWLEDGEMENTS

We acknowledge the Department of Physics, Indian institute of technology Delhi, New Delhi for providing the MPMS facility for magnetic measurements. This work is supported by Indo-French Centre for the Promotion of Advanced Research (IFCPAR/CEFIPRA) through grant no. 6508-2/2021 and Science and Engineering Research Board, Govt. of India through grant no. SPR/2021/000762.

## Supplemental Materials

This Supplemental materials includes

1. Materials and Methods
2. Modified Arrott-plots
3. Iteration method
4. Modified Iteration method
5. New proposals
6. Normalized slope plots for Ni
7. Field-dependent normalized slope and intercept plots for SC Gd
8. Modified Arrott-plots: theoretical and experimental results
9. Scaling results
10. Table of critical exponents (CEs) of standard 3D models, and the CE determined for Ni and SC Gd using various methods

### 1. Materials and Methods

#### a. Computational

Face centered cubic (FCC) Ni system was taken for the temperature- and field-dependent magnetization calculation. All the calculations were performed with the vampire software [30, 45] using the atomistic model simulations of magnetic Ni. The atomistic Landau–Lifshitz–Gilbert (LLG) equation was solved using the Heun integration scheme to calculate the magnetization curves [45]. The details about the LLG-Heun method can be found in [30, 45]. For the calculations for FCC Ni system, we take the following parameters: cluster size of  $20 \times 20 \times 20$  nm, unit cell size of 3.524 Å, atomistic spin moment  $\mu_S = 0.606\mu_B$ , exchange energy  $J_{ij} = 2.757 \times 10^{-26}$  J/link and we used magnetocrystalline anisotropy energy  $k_u = 0.0$  J/atom. For the LLG simulation, we use 50000 equilibrium steps and 500000 averaging steps. For all the calculations, we use the critical value of the Gilbert damping parameter equal to 1.0 and the computational time step equal to 0.1 fs [30, 45, 46]. We calculated temperature-dependent magnetization (M-T) with and without applying magnetic field. Finally, we converted the M-T isofields into field-dependent magnetization (M-H) isotherms and, thus, performed the theoretical investigation of the critical behavior of Ni system using the methods described below in sections 3 to 5.

#### b. Experimental

A single crystal (SC) of gadolinium (Gd) was grown using the Czochralski method [43] in a tetra-arc furnace (Technosearch Corporation, Tokyo, Japan). Approximately 7 grams of 99.9% pure Gd metal was placed on a water-cooled copper hearth inside the furnace. After evacuating the chamber to a vacuum of  $10^{-6}$  mBar, it was filled with high-purity argon gas. The Gd metal was melted using the conventional arc melting process. After the initial melt, the Gd was flipped and remelted under the same argon atmosphere. Gadolinium melts at around 1300 °C. A previously prepared polycrystalline Gd seed crystal was carefully introduced into the molten

Gd, causing local solidification around the seed. The seed crystal was then rapidly pulled at a speed of approximately 50 mm/h. The melt temperature was gradually increased to initiate the necking process, after which it was gradually decreased to widen the diameter of the growing crystal. Once steady-state conditions were achieved, the crystal was pulled at a steady speed of 10 mm/h for around 7 hours. The pulled ingot was subsequently aligned along its principal crystallographic directions using Laue diffraction and cut, using a wire EDM, along the basal plane and *c*-axis for anisotropic studies. Since the crystal was prone to oxidation in ambient conditions, precautions were taken to minimize its exposure to the atmosphere.

Temperature- and field-dependent magnetic measurements of SC Gd were carried out using Quantum Design magnetic properties measurement system (MPMS). The magnetic field was applied along [0001] direction.

*Temperature-dependent magnetization (M-T) scan in zero-field cooled warming (ZFCW) mode:* First, the sample was cooled to desired low-temperature, the M-T data were recorded with increasing temperature.

*M-T scan in field cooled warming (FCW) mode:* The sample was taken to high enough temperature in the paramagnetic region without applying field. One can guess the paramagnetic region from the recorded M-T in ZFCW mode. Further, after applying field, sample was cooled to desired low-temperature. The M-T data was recorded in warming mode.

*Field-dependent magnetization (M-H) scan:* Without applying field, the sample was cooled to desired low-temperature. Then, first-quadrant M-H isotherm was recorded in step (stable-field) mode. Next, the field was decreased to zero. Since, there is no hysteresis, so one can go directly from one temperature to other. That is how M-H isotherms were recorded at various temperatures in the vicinity of paramagnetic transition temperature,  $T_C$ .

### 2. Modified Arrott plots

In 1967, A. Arrott and J. E. Noakes [16] developed an empirical relation between magnetization ( $M$ ) and applied magnetic field ( $\mu_0 H$ ) using the critical exponents (CEs)  $\beta$  and  $\gamma$  as

$$(\mu_0 H/M)^{1/\gamma} = (T - T_C)/T_C + (M/M_1)^{1/\beta}, \quad (1)$$

where  $M_1$  is a temperature and field-dependent constant.  $T$  is the temperature at which the M-H isotherms are recorded. The plots of  $(\mu_0 H/M)^{1/\gamma}$  vs  $M^{1/\beta}$  is known as modified Arrott plots (MAPs).

### 3. Iteration method

The concept to develop the empirical relation 1 was to yield quasi straight line in the saturation magnetization region using a particular set of  $\beta$  and  $\gamma$  in the vicinity of  $T_C$ . To get appropriate  $\beta$  and  $\gamma$ , an iteration process was employed as follows:

For a given values of  $\beta$  and  $\gamma$ , the MAPs show quasi linear variation in the vicinity of  $T_C$ . A linear fit to a MAP,

in the saturation magnetization region, yields *slope* and *intercept*. Thus, on comparison with Eq. 1, one can estimate saturation magnetization,  $M_S(T)$  as

$$M_S(T) = (\textit{intercept})^\beta \text{ for } T < T_C, \quad (2)$$

and inverse of susceptibility,  $\chi_0^{-1}(T)$  as

$$\chi_0^{-1}(T) = \left( \frac{-\textit{intercept}}{\textit{slope}} \right)^\gamma \text{ for } T > T_C. \quad (3)$$

The estimated  $M_S(T)$  and  $\chi_0^{-1}(T)$  can be further fitted with

$$M_S(T) = M_0 | -\epsilon |^\beta \text{ for } \epsilon < 0 \quad (4)$$

and

$$\chi_0^{-1}(T) = h_0 / M_0 |\epsilon|^\gamma \text{ for } \epsilon > 0, \quad (5)$$

respectively. Here,  $\epsilon = \frac{T - T_C}{T_C}$  is the reduced temperature,  $M_0$  and  $h_0$  are constants. The above fittings (Eqs. 4 and 5) will yield new values of  $\beta$  and  $\gamma$ . Again, a new MAPs are constructed using the obtained *new* values of  $\beta$  and  $\gamma$ . Further, following the above processes (Eqs. 2 to 5), another set of  $\beta$  and  $\gamma$  are generated. The above processes will be repeated till the converged values of  $\beta$  and  $\gamma$  are achieved.

#### 4. Modified iteration method

Modified iteration method (MIM) [15] yields two sets of  $\beta$  and  $\gamma$  on either side of  $T_C$ . The process to estimate appropriate  $\beta$  and  $\gamma$  using MIM is as follows.

(i) First, including the M-H isotherm taken at  $T_C$ , make two sets of M-H isotherms: one for  $T \leq T_C$  and another one for  $T \geq T_C$ .

(ii) Take one set of M-H isotherms. Now, using  $\beta$  and  $\gamma$  of closest standard UC, estimate normalized slopes (NSs) as discussed in the main text. One should keep in mind—vary  $\beta$  and  $\gamma$  in such a way that the intercept, estimated from the linear fit to the MAPs at  $T_C$ , should pass through origin.

(iii) Take another values of  $\beta$  and  $\gamma$  (either by increasing or decreasing) in such a way that constructed NSs get closer to 1.

(iv) Stop the process when NSs become closest to 1 within error limit. This is how one set of  $\beta$  and  $\gamma$  will be estimated.

(v) Repeat steps (ii) to (iv) for the remaining set of M-H isotherms.

Thus, two separate sets of  $\beta$  and  $\gamma$  will be estimated.

### 5. New Proposals

#### a. The iterative process

In the main text, we propose a new method to get appropriate CEs of a system under investigation. The proposal correlates  $\beta$  and corresponding  $\gamma$  with  $\delta$  as follows

$$\gamma = \beta \times (\delta - 1), \quad (6)$$

where  $\delta$  is estimated from the M-H at  $T_C$  in different field ranges using the relation

$$M = M_0 (\mu_0 H)^{\frac{1}{\delta}}, \text{ at } T = T_C, \quad (7)$$

where  $M_0$  is a proportionality constant. Thus, the corresponding  $\gamma$  is obtained by putting  $\beta$  for a fix  $\delta$ , which is determined from the M-H at  $T_C$ , in Eq. 6. In this way, one can get a series of  $\beta$  and corresponding  $\gamma$ . Here, we have varied  $\beta$  with iteration number,  $n$  as  $\beta(n) = \beta_i + 0.001 \times n$ . In this way, one gets error in the value of  $\beta$  in third decimal place. The multiplication factor, 0.001 is depend on the choice of the user. Thus, we control the error in  $\beta$  manually. The error in  $\gamma$  depends on imposed error in  $\beta$  and the error appearing in  $\delta$ . It is obvious that one may get error in the magnetization during experiment. For the same, we put error in  $\beta$  up to 0.003. The reverse calculation using relation 6 is also true, *i.e.*, vary  $\gamma$  and determine corresponding  $\beta$  as  $\beta = \frac{\gamma}{\delta - 1}$ . In this way, one can control the error in  $\gamma$  manually and the error in  $\beta$  will depend on the imposed error in  $\gamma$  and the error appearing in  $\delta$ .

Finally, we construct the MAPs using the final CEs and by selecting the temperature range  $T \leq T_C$ . The linear fit to MAPs in the selected field-range yields slopes and intercepts. As observed and has been discussed in the main text, intercepts make crossover at  $T_C$ , which means, linear fit to MAP at  $T_C$  will pass through origin. After estimating  $NS$ , which is defined as  $NS = \frac{\text{slope of the linear fit to MAP at } T}{\text{slope of the linear fit to MAP at } T_C}$ , we determine average of  $NS$  ( $NS_{avg}$ ) as  $NS_{avg} = \frac{\sum_{i=1}^N (NS)_i}{N}$ , where  $i$  denotes the  $M-H$  isotherm at a given  $T$ , and  $N$  is the total number of the isotherms appearing in the calculation. As shown in Fig. S1, those values of  $\beta$  and corresponding  $\gamma$  (Eq. 6) are the appropriate for which  $NS_{avg} \sim 1$ . The details are mentioned in the main text.

#### b. The unconventional but simpler process

As shown in Fig. S1(a), the linear fit to  $NS_{avg}$  vs.  $n$ , yields slope= -0.002 and intercept= 1.016. The linearly fitted equation can be written as

$$NS_{avg.} = \text{slope} \times n + \text{intercept}. \quad (8)$$

Moreover, we have related  $\beta$  with  $n$  as  $\beta(n) = \beta_i + 0.001 \times n$ , where  $\beta_i = 0.400$  [Fig. S1(a)] for the selected field range. One can get appropriate  $n$  by putting  $NS_{avg} = 1$ , slope= -0.002 and intercept= 1.016 in Eq. 8. Thus, from the linear fit (Eq. 8), we get  $n = 8$  using which we determine  $\beta = 0.408$  which matches exactly as obtained from the conventional process.

In the unconventional approach, the iteration is not required, instead one can select a few set of  $\beta$  and  $\gamma$  correlated with Eq. 6, in such a way that the estimated  $NS_{avg}$  falls between 0.95 and 1.05. One can go for the selection of the  $NS_{avg}$  range from 0.9 to 1.1 or more,

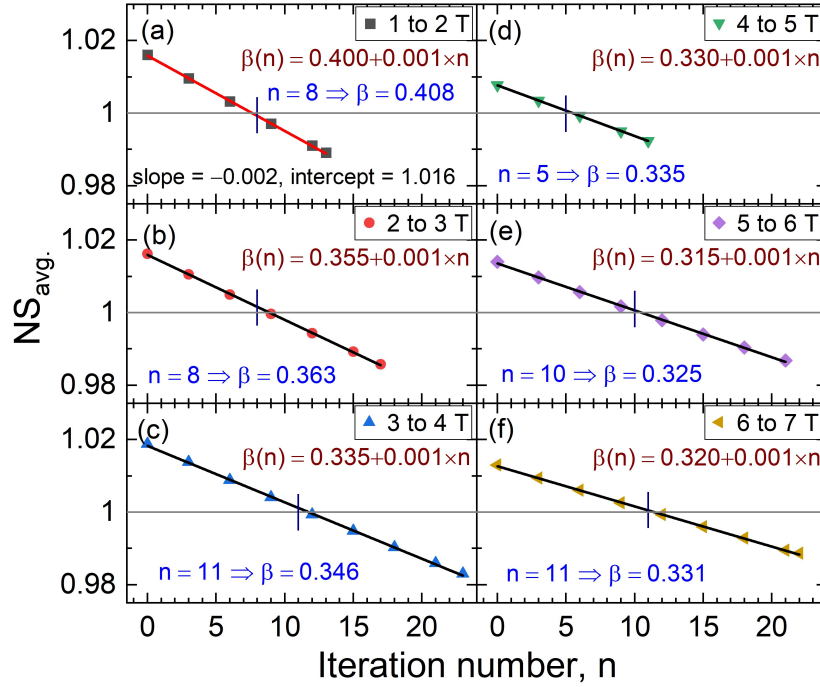


Figure S1. The variation of estimated  $NS_{avg}$ , which is defined as  $NS_{avg} = \frac{\text{Sum of NSs}}{\text{Total number of M-H isotherms}}$ , with iteration number ( $n$ ), which is related with  $\beta$  as  $\beta(n) = \beta_i + 0.001 \times n$ , where  $\beta_i$  is different for different field ranges as mentioned in respective figures as follows: (a) field-range from 1 to 2 T and  $\beta_i = 0.400$ , (b) field-range from 2 to 3 T and  $\beta_i = 0.355$ , (c) field-range from 3 to 4 T and  $\beta_i = 0.335$ , (d) field-range from 4 to 5 T and  $\beta_i = 0.330$ , (e) field-range from 5 to 6 T and  $\beta_i = 0.315$ , and (f) field-range from 6 to 7 T and  $\beta_i = 0.320$ . We get final  $\beta$ , when  $NS_{avg}$  is approximately equal to 1 at a particular value of  $n$  as mentioned in the respective figures.

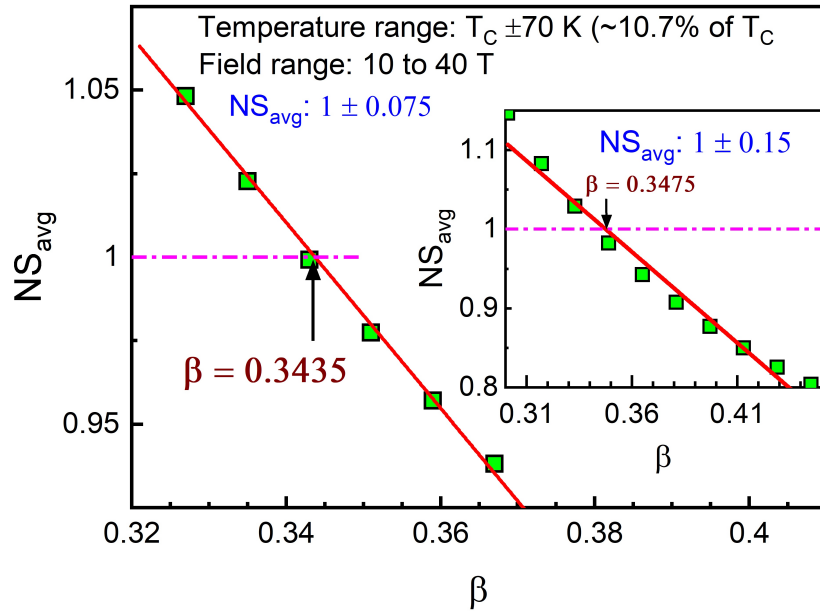


Figure S2. The variation of estimated  $NS_{avg}$  with  $\beta$ . The selected temperature range is  $T_C \pm 70$  K and the field range is from 10 to 40 T. The  $NS_{avg}$  vs.  $\beta$  plot show almost linear variation when values of  $NS_{avg}$  fall within  $1.00 \pm 0.05$ . The inset shows that  $NS_{avg}$  starts showing curvature when larger range of  $NS_{avg}$  is taken for analysis.



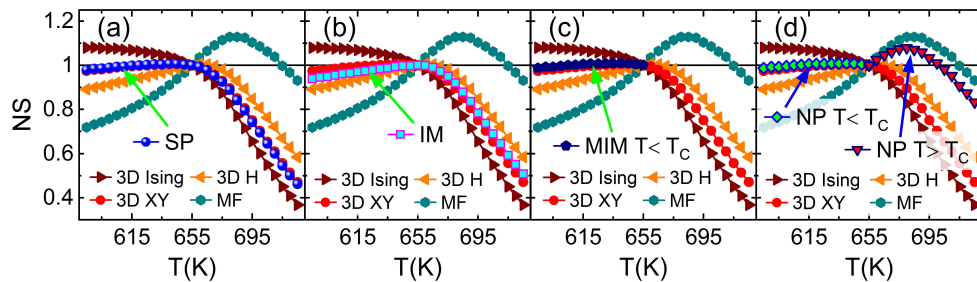


Figure S3. Normalized slope (NS) vs. temperature plots determined from the slope of the linear fit the modified Arrott-plots constructed using the critical exponents of standard UCs and the CEs determined using (a) standard procedure (SP), (b) iteration method (IM), (c) modified iteration method (MIM), and (d) our new proposal(s) (NP). The  $NS \sim 1$ , when estimated using the CEs determined using SP, MIM, and NP for  $T \leq T_C$ . The deviation of  $NS$  from 1 started above  $T_C$ . Also,  $NS$  deviates from 1 on either side of  $T_C$  when estimated using the CEs determined from IM.

but it should be noted that the  $NS_{\text{avg}}$  vs.  $\beta$  plot should show quasi-linear variation in the vicinity of  $NS_{\text{avg}} = 1$  as shown in Fig. S2 and Fig. 1(h) in the main text. Now, estimate  $NS_{\text{avg}}$  for the selected set of  $\beta$  and corresponding  $\gamma$ , and do  $NS_{\text{avg}}$  vs.  $\beta$  plot. Here, one can take a minimum sets of  $\beta$  and corresponding  $\gamma$  to perform a linear fit. Our recommendation is to select at least three set of  $\beta$  and corresponding  $\gamma$  in such a way the estimated  $NS_{\text{avg}}$  falls on both side of  $NS_{\text{avg}} = 1$ . Finally, the linear fit to the plot will yield *slope* and *intercept*. Now, using the relations,

$$\beta = \frac{1 - \text{intercept}}{\text{slope}} \quad (9)$$

and

$$\gamma = \frac{1 - \text{intercept}}{\text{slope}} \times (\delta - 1), \quad (10)$$

the appropriate respective values of  $\beta$  and  $\gamma$  can be determined easily. We have tested this concept for the field range 10 to 40 T as shown in Fig. S2. As shown, from the intersection point of the linear fit to data and the horizontal line drawn passing through  $NS_{\text{avg}} = 1$ , we directly get  $\beta = 0.3435$ . By inserting the determined *slope* and *intercept* (Fig. S2) in relation 9, we get  $\beta \approx 0.343$ , which matches exactly as determined using our proposed conventional iteration process and SP. However, when the range of  $NS_{\text{avg}}$  is increased up to  $1.00 \pm 0.15$  [Inset of Fig. S2], the determined value of  $\beta \approx 0.347$  starts deviating away. And  $NS_{\text{avg}}$  vs.  $\beta$  started showing curvature.

## 6. Normalized slope plots for Ni

Figure S3 shows the normalized slope (NS) vs. temperature plots determined from the slope of the linear fit the modified Arrott-plots constructed using the CEs of standard UCs and the CEs determined using standard procedure (SP).

## 7. Field-dependent normalized slope and intercept plots for SC Gd

The linear fits to MAPs, constructed using the CEs of standard UCs and the CEs determined using our new

proposal (NP) [Fig. S1], yield slopes and intercepts. Figure S4 represents the variation of NSs with temperature (defined above and in the main text) estimated using the CEs of standard UCs and the CEs determined using NP. As shown in Fig. S4, NSs make the first indication that the critical behavior of SC should belong to either 3D XY UC or 3D Heisenberg UC in low-field range. But, the determined CEs differ the guess made by NS plots. The primary guess made by the NS plots for higher field range [Figs. S4(b) to S4(f)], which is 3D Ising UC, do not depict the full physics of the system. The NS plots, constructed using the CEs determined using NP, are always closest to 1, which is the indication of the appropriate CEs. The determined CEs [Fig. S1] do not belong to a single UC. This is the indication that one cannot depict the emerging physics directly from the NS plots using the CEs of standard UCs. One need to perform the critical analysis to reveal the correct physics.

Figure S5 represents the variation of Intercepts with temperature (defined above and in the main text) estimated using the CEs of standard UCs and the CEs determined using NP. Let  $T_1$  is the temperature where the intercepts for short-range UCs (3D Heisenberg, 3D Ising and 3D XY) make crossover and has very less variation with applied field range. Let  $T_2$  is the temperature where the intercepts for long-range MF UC make crossover and has significant variation with applied field range. We have corroborated in the main text that the variation of  $T_2$  indicate the dominance of long-range coupling in low-field range which eventually gets weaker with applied field resulting in the coexistence of both long- and short-range coupling in the high-field range. The intercepts, estimated using the CEs determined using NP, make crossover at  $T_C$ .

## 8. Modified Arrott plots: theoretical and experimental results

Figure S6 represents the MAPs constructed for Ni using the CEs of standard UCs [Figs. S6(a) to S6(d)] and the CEs determined by standard process (SP) [Fig. S6(e)], iteration method (IM) [Fig. S6(f)], MIM [Fig.

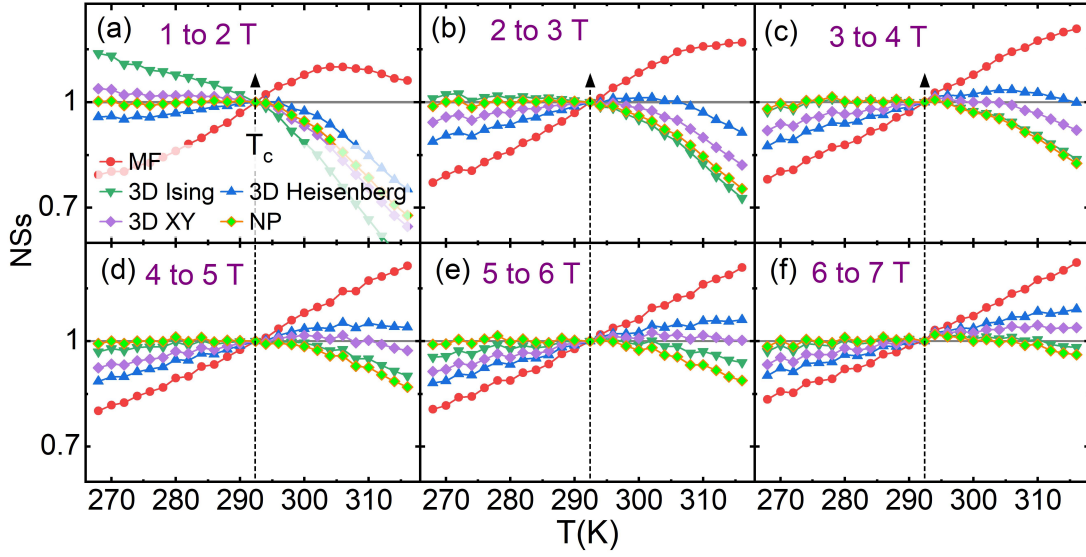


Figure S4. Normalized slopes (NSs) vs. temperature plots determined from the slope of the linear fit the modified Arrott-plots constructed using the critical exponents of standard UCs and the CEs determined using the new proposal for the field range (a) 1 to 2 T, (b) 2 to 3 T, (c) 3 to 4 T, (d) 4 to 5 T, (e) 5 to 6 T and (f) 6 to 7 T.

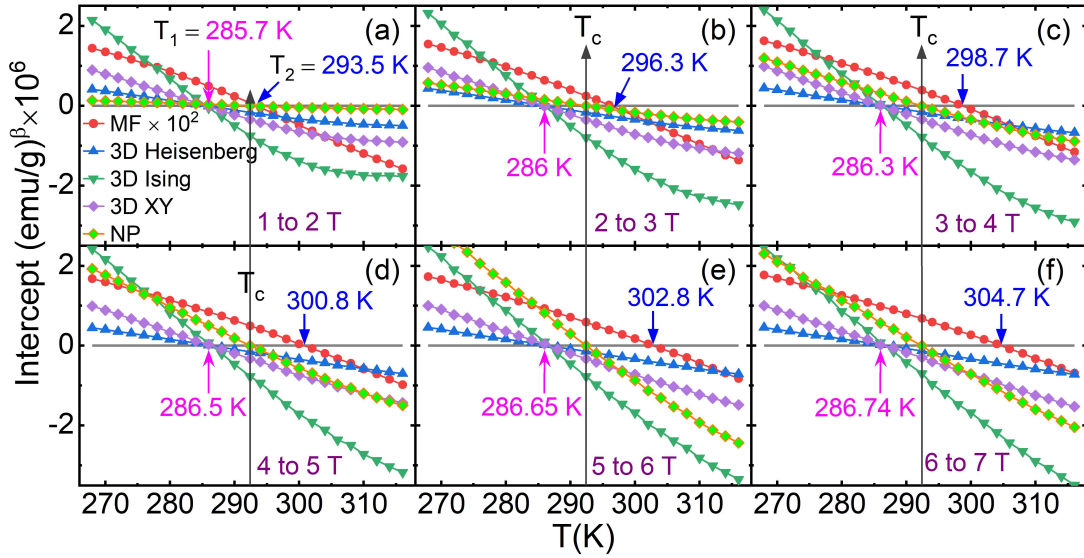


Figure S5. Intercepts vs. temperature plots determined from the intercept of the linear fit the modified Arrott-plots constructed using the critical exponents of standard UCs and the CEs determined using the new proposal for the field range (a) 1 to 2 T, (b) 2 to 3 T, (c) 3 to 4 T, (d) 4 to 5 T, (e) 5 to 6 T and (f) 6 to 7 T.

S6(g)], and NP [Fig. S6(h)] for the critical analysis. As one can see the MAPs constructed using the CEs determined from IM show slightly non-co-linear variation which is also evidenced from the NS plots [Fig. S3(b)] which show deviation from 1. While the MAPs constructed using the CEs determined from MIM and NP show quasi linear variation for all the isotherms for below  $T_C$ . This is also evidenced from the NS plots [Figs. S3(c) and S3(d)] which is close to 1 for below  $T_C$ . As observed, the linear variation of MAPs, constructed us-

ing the CEs determined from MIM and NP, for above  $T_C$  show that the field-range of the linear variation decreases with increasing temperature. This investigation yields two points: (i) one should do the critical analysis in low-temperature and high-field ranges for above  $T_C$ , and (ii) to perform critical analysis in the whole temperature range, the field-range should be varied to acquire the linear variation in the MAPs.

Figure S7 represents the MAPs constructed for SC Gd system using the CEs of standard UCs [Figs. S7(a) to

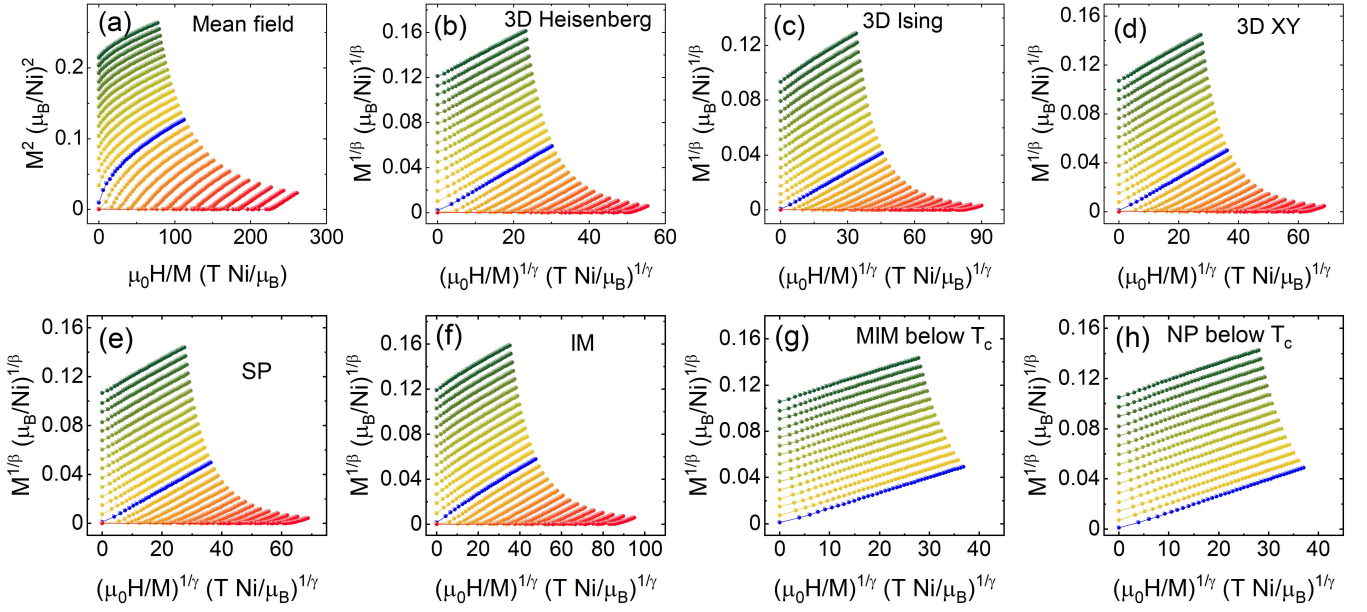


Figure S6. The modified Arrott-plots (MAPs) constructed using the  $\beta$  and  $\gamma$  of (a-d) standard universality classes, (e) SP, (f) IM, (g) MIM, and (h) the new proposal.

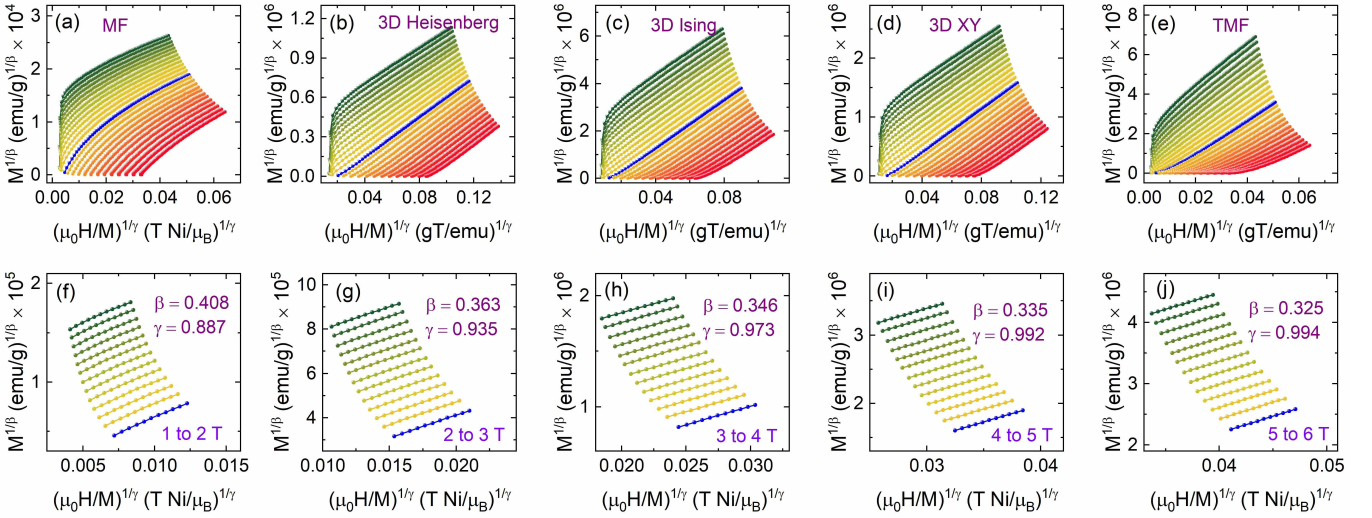


Figure S7. (a) to (e) The modified Arrott-plots (MAPs) constructed using the  $\beta$  and  $\gamma$  of standard universality classes for Gd. (f) to (j) The MAPs constructed using the determined  $\beta$  and  $\gamma$  from the proposed method for below  $T_C$  and in different field ranges as mentioned.

S7(e)] and the CEs determined by the NP for different field ranges [Figs. S7(f) to S7(j)] for below  $T_C$ . The MAPs, constructed using the CEs of standard UCs, indicate that the critical behavior of SC Gd should belong to one of the short-range standard UCs. The MAPs, constructed using the CEs determined by NP, for the field range 1 to 2 T show significant but smaller deviation from quasi-linear variation. The MAPs for higher field-ranges show almost quasi-linear variation. This is the indication that the results obtained for the field range 1 to 2 T may be ambiguous. The critical analysis for above  $T_C$

have been ignored due to the reasons discussed in the main text while performing theoretical investigation on Ni system.

## 9. Scaling results

The scaling equation of state, for magnetic systems, takes the form [5, 47]

$$\frac{\mu_0 H}{M^{1/\delta}} = \tilde{h}\left(\frac{\epsilon}{M^{1/\beta}}\right), \quad (11)$$

where  $\tilde{h}(x)$  is the scaling function. Thus, the relation 11 states that for appropriate CEs and  $T_C$ , the plots

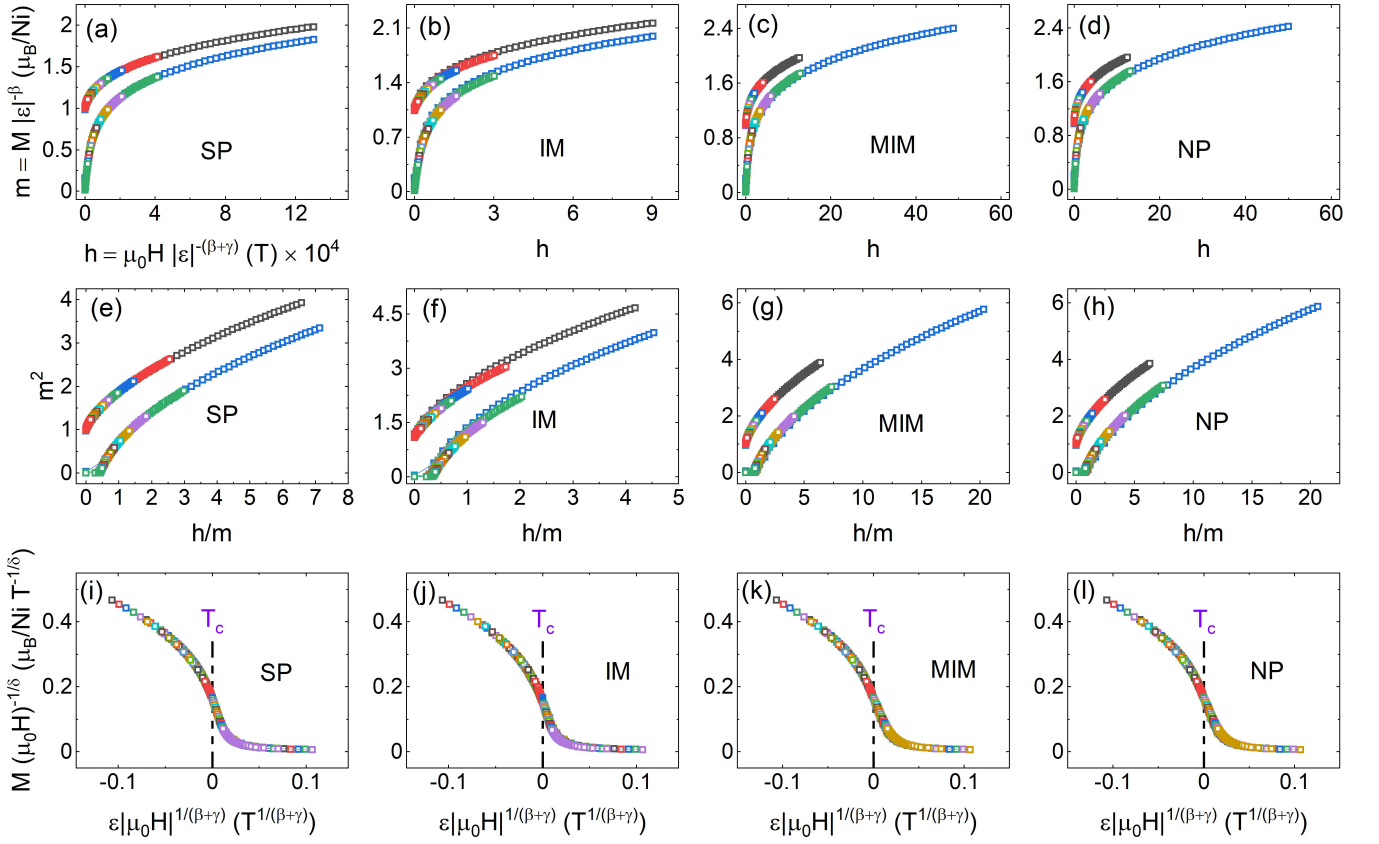


Figure S8. (a) to (d) Scaling of the M-H isotherms using the relation 12 and the CEs determined using standard process (SP), iteration method (IM), modified IM (MIM) and our new proposal (NP) as mentioned in the respective figures. The scaling yields renormalized magnetization,  $m = M|\epsilon|^{-\beta}$  and renormalized field  $h = \mu_0 H |\epsilon|^{-(\beta+\gamma)}$ . (e) to (h) The renormalized Arrott-plots (RAPs),  $m^2$  vs.  $h/m$ , for the CEs determined from SP, IM, MIM and NP as mentioned in the respective figures. (i) to (l) Scaling of the M-H isotherms using the relation 11 and the CEs determined using SP, IM, MIM and NP as mentioned in the respective figures.

of  $M(\mu_0 H)^{1/\delta}$  vs.  $\epsilon(\mu_0 H)^{-\frac{1}{\beta+\gamma}}$  should corresponds to a universal curve onto which all the isotherms collapse. The Eq. 11 may be formally converted as

$$M(\mu_0 H, \epsilon)|\epsilon|^{-\beta} = f_{\pm} \left( \frac{\mu_0 H}{\epsilon^{\beta+\gamma}} \right), \quad (12)$$

where  $f_+$  and  $f_-$  are defined for  $T > T_C$  and  $T < T_C$ , respectively. The relation 12 states – for appropriate values of  $\beta$  and  $\gamma$ , the plots of renormalized magnetization,  $m = M(H, \epsilon)|\epsilon|^{-\beta}$  vs. renormalized field,  $h = \mu_0 H |\epsilon|^{-(\beta+\gamma)}$  should correspond to collapse of the isotherms on two separate universal curves for below and above  $T_C$ . Equation 12 is most commonly used relation to verify the appropriateness of the obtained CEs. It has been proven [15] that these scaling relations (Eqs. 11 and 12) can absorb significantly large errors appearing in the determination of CEs. So, a new and appropriate relation is needed to check the reliability of determined CEs. However, Widom relation,  $\delta = 1 + \frac{\gamma}{\beta}$ , may be used as a primary tool to check the reliability and accuracy of

determined CEs using various methods.

Figures S8(a) to S8(d) show the plots of  $m$  vs.  $h$  constructed using the CEs determined by SP, IM, MIM and NP for Ni system. As one can see clearly that the  $m$  vs.  $h$  plots using the CEs determined by IM [Fig. S8(b)] show maximal deviation from overlapping on two separate isotherms. The  $m$  vs.  $h$  using the CEs determined by SP [Fig. S8(a)] have perfect collapse on two universal curves for the whole range of the M-H isotherms. Similar perfect collapse on two universal curves for the whole range of the M-H isotherms have been observed using the CEs determined by MIM [Fig. S8(c)] and NP [Fig. S8(d)] for below  $T_C$ . We have used the same CEs, determined by MIM and NP for below  $T_C$ , to construct the  $m$  vs.  $h$  plots for above  $T_C$ , which show slight deviation from collapsing on a universal curve. Figures S8(e) to S8(h) are the renormalized Arrott-plots (RAPs) constructed using the CEs determined by SP, IM, MIM and NP. The perfect overlapping is closely observable for the CEs determined by SP, and MIM and NP for below  $T_C$ . The RAPs constructed using the CEs determined by IM,

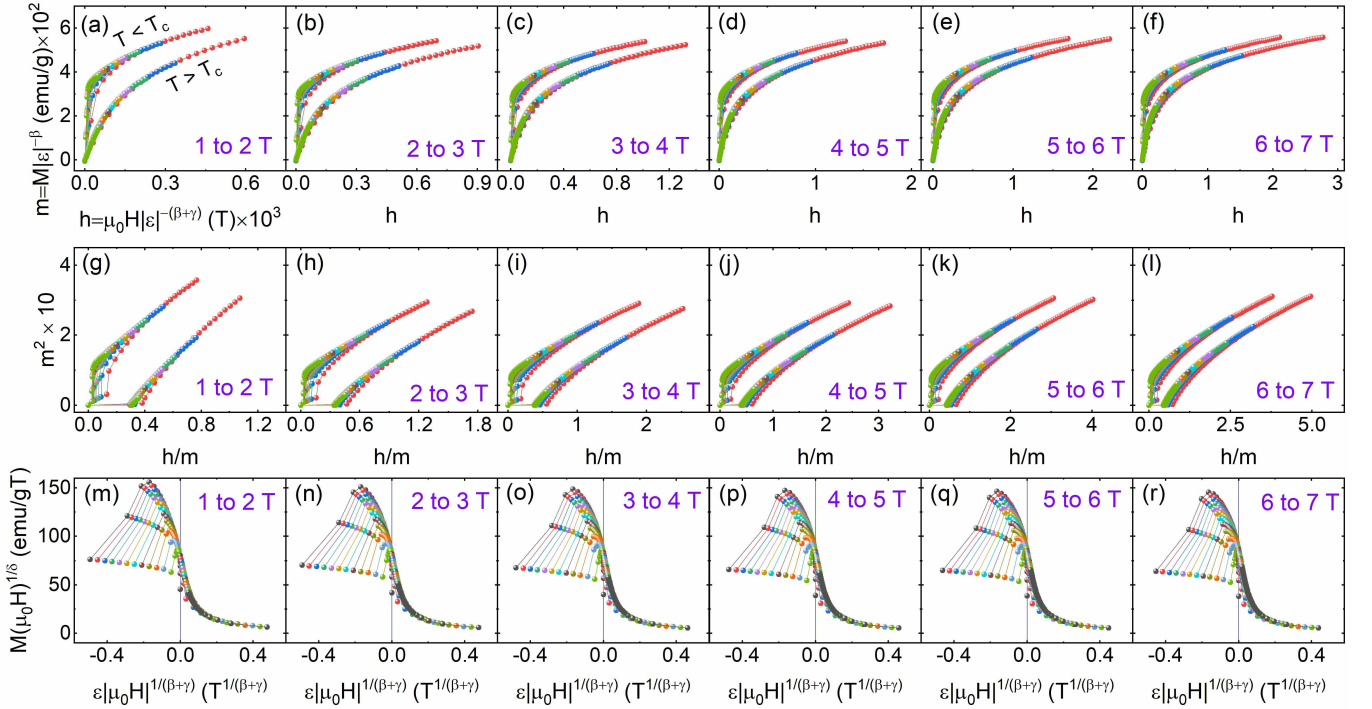


Figure S9. (a) to (f) Scaling of the M-H isotherms using the relation 12 and the CEs determined using our new proposal (NP) for different field-ranges as mentioned in the respective figures. The scaling yields renormalized magnetization,  $m = M|\epsilon|^{-\beta}$  and renormalized field,  $h = \mu_0 H |\epsilon|^{-(\beta+\gamma)}$ . (g) to (l) The renormalized Arrott-plots (RAPs),  $m^2$  vs.  $h/m$ , for the CEs determined from NP for the different field-ranges as mentioned in the respective figures. (m) to (r) Scaling of the M-H isotherms using the relation 11 and the CEs determined using NP for the different field-ranges as mentioned in the respective figures.

MIM for above  $T_C$  and NP for above  $T_C$  show slightly large deviation from collapsing on universal curve. These are the indication that the CEs determined using SP, and MIM and NP for below  $T_C$  are appropriate to reveal the properties of a system under investigation. In fact, the CEs determined from the above three mentioned methods (SP, MIM and NP) match significantly to each other within error limit. The details have been discussed in the main text. However, no concrete conclusion can be made from the use of relation 11 because the constructed plots using the CEs determined by all methods overlap significantly onto a single universal curves as shown in Figs. S8(i) to S8(l). From these investigations, One important information is coming out – the overlapping of all the isotherms on universal curves for entire field-range is the indication of the existence of single exchange coupling in the system, which was intentionally incorporated during simulation.

Figure S9 represents the scaling plots and RAPs for SC Gd. One should note that the critical analysis on SC Gd have been carried out only for below  $T_C$  but we have plotted the above  $T_C$  isotherms also using the same CEs as determined for below  $T_C$ . The plots shown in Fig. S9, have been constructed using the CEs determined by NP. The  $m$  vs.  $h$  plots show nice overlapping in the field-ranges which were used to determine CEs for below

$T_C$ . However, in the low field range (approximately below 0.5 T) the  $m$  vs.  $h$  plots [Figs. S9(a) to S9(f)] show deviations from collapsing on the universal curves. In the similar fashion, the RAPs [Figs. S9(g) to S9(l)] also show overlapping in the high field range while deviations are observable in the low field range. The scaling plots [Figs. S9(m) to S9(r)], constructed using the relation 11, also show significant deviations in the low-field range mainly below  $T_C$ . The reported scaling results using Eq. 11 do not show deviation from collapsing on single universal curve. The reason behind this could be the skipping of the low-field data. However, from the deviation in the low-field region, we state that this is the signature of the competing energies along with symmetric exchange interaction in SC Gd. The detail discussions have been given in the main text.

**10. Table of critical exponents of standard 3D models, and the critical exponents determined for Ni and SC Gd estimated using various methods**

Table I. The list of CEs ( $\beta$ ,  $\gamma$ ,  $\delta$  and  $\alpha$ ) of standard 3D universality classes and the CEs determined using various methods as discussed above and presented in the main text. *Ref.:* References, *Tech:* Techniques, *RG:* renormalization group, *TMF:* tricritical mean-field, *H:* Heisenberg, *ME:* magnetic entropy, *PM:* proposed method, *Expt.:* experiment, *d:* space dimensionality, and *n:* spin dimensionality.

Model/ Sample	Ref/ Field-range	Method	Critical Exponents				Dimensionality	
			$\beta$	$\gamma$	$\delta$	$\sigma$	$d$	$n$
Mean-field	[19, 47]	Theory	0.500	1.000	3.000	1.500	3	–
TMF	[19]	Theory	0.250	1.000	5.000	1.500	3	–
3D Ising	[19, 47]	Theory	0.325	1.237	4.800	1.960	3	1
3D XY	[19, 47]	Theory	0.345	1.316	4.800	1.960	3	2
3D H	[19, 47]	Theory	0.365	1.386	4.800	1.960	3	3
Ni	This Paper	Theory (SP)	0.344(2)	1.315(8)	4.823(15)	1.920(8)	3	2
Ni	This Paper	Theory (IM)	0.362(1)	1.222(10)	4.376(37)	1.877(14)	3	1
Ni	This Paper	Theory (MIM)	0.343(3)	1.309(8)	4.816(57)	1.931(8)	3	2
Ni	This Paper	Theory (NP)	0.342(3)	1.307(12)	4.822(69)	1.911(13)	3	2
SC Gd	1 to 2 T	Expt. (NP)	0.408(3)	0.887(14)	3.174(24)	1.247(49)	3	–
SC Gd	2 to 3 T	Expt. (NP)	0.363(3)	0.935(10)	3.576(13)	1.377(22)	3	–
SC Gd	3 to 4 T	Expt. (NP)	0.346(3)	0.973(9)	3.811(10)	1.453(16)	3	–
SC Gd	4 to 5 T	Expt. (NP)	0.335(3)	0.992(9)	3.961(11)	1.487(15)	3	–
SC Gd	5 to 6 T	Expt. (NP)	0.325(3)	0.994(8)	4.060(7)	1.490(13)	3	–
SC Gd	6 to 7 T	Expt. (NP)	0.331(3)	1.055(10)	4.186(12)	1.583(14)	3	–

\* Harish.chandr.chauhan@physics.iitd.ac.in;  
pintu@physics.iitd.ac.in

- [1] C. Zener and R. R. Heikes, *Exchange Interactions*, *Rev. Mod. Phys.* **25**, 191 (1953).
- [2] P. Wahl, P. Simon, L. Diekhoner, V. S. Stepanyuk, P. Bruno, M. A. Schneider, and K. Kern, *Exchange Interaction between Single Magnetic Adatoms* *Phys. Rev. Lett.* **98**, 056601 (2007).
- [3] H. C. Chauhan, B. Kumar, J. K. Tiwari, and S. Ghosh, *Multiple phases with a tricritical point and a Lifshitz point in the skyrmion host Cu<sub>2</sub>OSeO<sub>3</sub>* *Phys. Rev. B* **100**, 165143 (2019).
- [4] M. E. Fisher, *The renormalization group in the theory of critical behavior*, *Rev. Mod. Phys.* **46**, 597 (1974).
- [5] H. E. Stanley, *Scaling, universality, and renormalization: Three pillars of modern critical phenomena*, *Rev. Mod. Phys.* **71**, S358 (1999).
- [6] Y. Liu, V. N. Ivanovski, and C. Petrovic, *Critical behavior of the van der Waals bonded ferromagnet Fe<sub>3-x</sub>GeTe<sub>2</sub>* *Phys. Rev. B* **96**, 144429 (2017).
- [7] P. Bisht and R. N. Mahato, *Investigation of magnetic properties and colossal magnetoresistance in nanocrystalline doped manganite*, *J. Phys. Condens. Matter* **35**, 475802 (2023).
- [8] J. Goldenhuys and D. H. Wiid, *RKKY interaction and conduction electron polarisation*, *J. Phys. Condens. Matter* **8**, 2021 (1978).
- [9] F. Parhizgar, H. Rostami, and R. Asgari, *Indirect exchange interaction between magnetic adatoms in monolayer MoS<sub>2</sub>*, *Phys. Rev. B* **87**, 125401 (2013).
- [10] A. Scheie, P. Laurell, P. A. McClarty, G. E. Granroth, M. B. Stone, R. Moessner, and S. E. Nagler, *Spin-exchange Hamiltonian and topological degeneracies in elemental gadolinium*, *Phys. Rev. B* **105**, 104402 (2022).
- [11] H. C. Chauhan, B. Kumar, and S. Ghosh, *Origin of metamagnetism in skyrmion host Cu<sub>2</sub>OSeO<sub>3</sub>*, *Sci. Rep.* **12**, 15971 (2022).
- [12] J. K. Tiwari, H. C. Chauhan, B. Kumar, and S. Ghosh, *3d-Ising like ferromagnetism in skyrmionic-bubbles host infinite-layer La<sub>0.825</sub>Sr<sub>0.175</sub>MnO<sub>3</sub> manganite perovskite*, *J. Phys. Condens. Matter* **32**, 195803 (2020).
- [13] M. Phan, V. Franco, N. Bingham, H. Srikanth, N. Hur, and S. Yu, *Tricritical point and critical exponents of La<sub>0.7</sub>Ca<sub>0.3-x</sub>Sr<sub>x</sub>MnO<sub>3</sub> (x = 0, 0.05, 0.1, 0.2, 0.25) single crystals*, *J. Alloys Compd.* **508** 238 (2010).
- [14] F. Leonard and B. Delamotte, *Critical Exponents Can Be Different on the Two Sides of a Transition: A Generic Mechanism*, *Phys. Rev. Lett.* **115**, 200601 (2015).
- [15] H. C. Chauhan, B. Kumar, A. Tiwari, J. K. Tiwari, and S. Ghosh, *Different Critical Exponents on Two Sides of a Transition: Observation of Crossover from Ising to Heisenberg Exchange in Skyrmion Host Cu<sub>2</sub>OSeO<sub>3</sub>*, *Phys. Rev. Lett.* **128**, 015703 (2022).
- [16] A. Arrott and J. E. Noakes, *Approximate Equation of State For Nickel Near its Critical Temperature*, *Phys. Rev. Lett.* **19**, 786 (1967).
- [17] K. Ghosh, C. J. Lobb, R. L. Greene, S. G. Karabashiev, D. A. Shulyatev, A. A. Arsenov, and Y. Mukovskii, *Critical Phenomena in the Double-Exchange Ferromagnet La<sub>0.7</sub>Sr<sub>0.3</sub>MnO<sub>3</sub>* *Phys. Rev. Lett.* **81**, 4740 (1998).
- [18] A. Bhattacharya, A. Ahmed, S. DuttaGupta, and I. Das, *Critical behavior and phase diagram of skyrmion-hosting material Co<sub>3.6</sub>Fe<sub>4.4</sub>Zn<sub>8</sub>Mn<sub>4</sub> probed by anomalous Hall effect*, *J. Alloys Compd.* **960** 170274 (2023).
- [19] D. Kim, B. L. Zink, F. Hellman, and J. M. D. Coey, *Critical behavior of La<sub>0.75</sub>Sr<sub>0.25</sub>MnO<sub>3</sub>*, *Phys. Rev. B* **65**, 214424 (2002).

- [20] S. Srinath and S. N. Kaul, *Static universality class for gadolinium*, *Phys. Rev. B* **60**, 12166 (1999).
- [21] G. S. Collins, A. R. Chowdhury, and C. Hohenemser, *Observation of isotropic critical spin fluctuations in Gd*, *Phys. Rev. B* **33**, 4747 (1986).
- [22] D. J. W. Geldart, P. Hargraves, N. M. Fujiki, and R. A. Dunlap, *Anisotropy of the critical magnetic susceptibility of gadolinium*, *Phys. Rev. Lett.* **62**, 2728 (1989).
- [23] N. T. Dang, D. P. Kozlenko, D. N. Petrov, J. Cwik, G. Kim, W. H. Shon, J. S. Rhyee, S. C. Yu, and P. T. Long, *Magnetic field driven critical behavior in bulk Gd*, *J. Appl. Phys.* **125**, 153903 (2019).
- [24] J. S. Kouvel and M. E. Fisher, *Detailed Magnetic Behavior of Nickel Near its Curie Point*, *Phys. Rev.* **136**, A1626 (1964).
- [25] V. Franco, J. Blazquez, and A. Conde, *Field dependence of the magnetocaloric effect in materials with a second order phase transition: A master curve for the magnetic entropy change*, *Appl. Phys. Lett.* **89**, 222512 (2006).
- [26] M. E. Fisher, S.-k. Ma, and B. G. Nickel, *Critical Exponents for Long-Range Interactions*, *Phys. Rev. Lett.* **29**, 917 (1972).
- [27] J. Sak, *Recursion Relations and Fixed Points for Ferromagnets with Long-Range Interactions*, *Phys. Rev. B* **8**, 281 (1973).
- [28] J. Sak, *Low-temperature renormalization group for ferromagnets with long-range interactions*, *Phys. Rev. B* **15**, 4344 (1977).
- [29] J. K. Tiwari, B. Kumar, H. C. Chauhan, and S. Ghosh, *Critical scaling and magnetic phase diagram of biskyrmion host quasi-two-dimensional  $\text{La}_{1.37}\text{Sr}_{1.63}\text{Mn}_2\text{O}_7$  bi-layer manganite*, *J. Magn. Magn. Mater.* **535**, 168020 (2021).
- [30] R. F. L. Evans, W. J. Fan, P. Chureemart, T. A. Ostler, M. O. A. Ellis, and R. W. Chantrell, *Atomistic spin model simulations of magnetic nanomaterials*, *J. Phys. Condens. Matter* **26**, 103202 (2014).
- [31] See supplemental materials for discussion on materials and methods, modified Arrott-plots, iteration method, modified iteration method, new proposals, the normalized slope plots for Ni, the field-dependent normalized slope and intercept plots for SC Gd, the modified Arrott-plots constructed for theoretical and experimental results, the scaling results, the table of critical exponents of standard 3D models and the critical exponents determined for Ni and SC Gd using various methods.
- [32] M. E. Fisher, *The theory of equilibrium critical phenomena*, *Rep. Prog. Phys.* **30**, 615 (1967).
- [33] B. Widom, *The critical point and scaling theory*, *Physica* **73**, 107 (1974).
- [34] A. Pelissetto and E. Vicari, *Critical phenomena and renormalization-group theory* *Phys. Rep.* **368**, 549 (2002).
- [35] E. Anderson, S. Arajs, A. Stelmach, B. Tehan, and Y. Yao, *Critical exponent  $\beta$  for nickel and nickel-copper alloys*, *Phys. Lett. A* **36**, 173 (1971).
- [36] J. C. Le Guillou and J. Zinn-Justin, *Critical Exponents for the n-Vector Model in Three Dimensions from Field Theory*, *Phys. Rev. Lett.* **39**, 95 (1977).
- [37] J. C. Le Guillou and J. Zinn-Justin, *Critical exponents from field theory* *Phys. Rev. B* **21**, 3976 (1980).
- [38] M. Seeger, S. N. Kaul, H. Kronmüller, and R. Reisser, *Asymptotic critical behavior of Ni* *Phys. Rev. B* **51**, 12585 (1995).
- [39] L. Oroszlány, A. Deak, E. Simon, S. Khmelevskiy, and L. Szunyogh, *Magnetism of Gadolinium: A First-Principles Perspective* *Phys. Rev. Lett.* **115**, 096402 (2015).
- [40] B. Frietsch, J. Bowlan, R. Carley, M. Teichmann, S. Wienholdt, D. Hinzke, U. Nowak, K. Carva, P. M. Oppeneer, and M. Weinelt, *Disparate ultrafast dynamics of itinerant and localized magnetic moments in gadolinium metal* *Nat. Commun.* **6**, 8262 (2015).
- [41] L. M. Sandratskii and J. Kübler, *Local Magnetic Moments of Conduction Electrons in Gadolinium* *Europhys. Lett.* **23**, 661 (1993).
- [42] S. Khmelevskiy, I. Turek, and P. Mohn, *Interaction between itinerant and localized electrons at finite temperatures in pure hcp Gd: an ab initio DLM study*, *Phys. B Condens. Matter* **359-361**, 145 (2005).
- [43] P. E. Tomaszewski, *Jan Czochralski—father of the Czochralski method*, *J. Cryst. Growth* **236**, 1 (2002).
- [44] S. Y. Dan'kov, A. M. Tishin, V. K. Pecharsky, and K. A. Gschneidner, *Magnetic phase transitions and the magnetothermal properties of gadolinium*, *Phys. Rev. B* **57**, 3478 (1998).
- [45] R. F. L. Evans, U. Atxitia, and R. W. Chantrell, *Quantitative simulation of temperature-dependent magnetization dynamics and equilibrium properties of elemental ferromagnets* *Phys. Rev. B* **91**, 144425 (2015).
- [46] O. Pastukh, M. Kac, S. Pastukh, D. Kuzma, M. Zelen, M. Krawczyk, and u. Laskowski, *Magnetic Behavior of the Arrays of Iron Cylindrical Nanostructures: Atomistic Spin Model Simulations* *Crystals* **13**, 10.3390/cryst13030537 (2023).
- [47] S. N. Kaul, *Static critical phenomena in ferromagnets with quenched disorder*, *J. Magn. Magn. Mater.* **53**, 5 (1985).